Supplementary Material

Effects of human atrial ionic remodelling by β-blocker therapy on mechanisms of AF: a computer simulation

Sanjay R Kharche[1,2], Tomas Stary[1], Michael A Colman[2], Irina V Biktasheva[3], Antony J Workman[4]*, Andrew C Rankin[5], Arun V Holden[6], Henggui Zhang[2]*

[1]College of Engineering, Mathematics, and Physical Sciences, University of Exeter, UK
[2]Biological Physics Group, School of Physics and Astronomy, University of Manchester, UK
[3]Department of Computer Sciences, University of Liverpool, UK
[4]Institute of Cardiovascular and Medical Sciences, University of Glasgow, UK
[5]School of Medicine, University of Glasgow, UK
[6]School of Biomedical Sciences, University of Leeds, UK

Correspondence*:
Prof. Henggui Zhang
Biological Physics Group, School of Physics and Astronomy, The University of Manchester, Manchester M13 9PL
Email : Henggui.Zhang@manchester.ac.uk
Tel : +44 (0) 161-306-3966
Fax : +44 (0) 161-275-4297

AND

Dr Antony J Workman
Institute of Cardiovascular and Medical Sciences, College of Medical, Veterinary and Life Sciences, University of Glasgow, 126 University Place, Glasgow G12 8TA
Email: Antony.Workman@glasgow.ac.uk
Tel.:+44 (0) 141-330-3451

S1. Methods

S1.1 Cellular excitation models

Three biophysically detailed models of human atrial cell APs, by Courtemanche et al. [1] (CRN), Grandi et al. [2] (Grandi), and Koivumaki et al. [3] (KT) were used. The CRN model (21 variables) has a spike-and-dome shaped type 1 AP. The Grandi model (41 variables) has a detailed Ca^{2+} handling mechanism and reproduces the type 3 triangular AP morphology seen in human atrial myocytes (see Dawodu et al. [4]). While the Grandi model presumes a level of t-tubule organisation in atrial myocytes [2], the KT model (43 variables) is based on heterogeneous intracellular Ca^{2+} dynamics in atrial myocytes lacking t-tubule structures.

S1.2 Ionic current alterations due to chronic β-blocker remodelling in atrial cells

The experimental study by Marshall et al. [5] quantified the effects of chronic β-blocker treatment in patients on human atrial cellular electrophysiology as a reduction of I_{K1} conductance (g_{K1}) by 34%, and I_{to} conductance (g_{to}) by 41%. These alterations were incorporated into the CRN and Grandi cell models. As seen in the experimental and model simulated current-voltage (I-V) relationships for I_{K1} and I_{to} under control and β-blocker conditions (Supplementary Material, Figure S1), the densities of the two currents in the KT model (Figure S1, D) are markedly different from our experimental data. Given the large I_{K1} density in the KT model, a 34% reduction of g_{K1} caused the model AP to become unstable and without repolarisation. Therefore a smaller reduction of g_{K1} (by 10%) along with a 41% reduction of g_{to} was incorporated into the KT model. The 10% reduction of g_{K1} in the KT model was the maximum reduction which still gave stable APs. Such alterations in the KT model gave similar relative AP prolongation to that produced using the Grandi model. Cell APs were evoked using standard pacing protocols [6] at a rate of 1 Hz for 100 beats, and resting potential (RP), AP duration at 90% repolarisation (APD_{90}), APD_{30}, overshoot potential (OS), maximal upstroke velocity (dV/dt_{max}) were computed from steady oscillations. Triangulation of APs [7] was defined as:

$$triangulation = (V\_apd90 - V\_apd30)/(t\_apd90 - t\_apd30),$$

where V_apd90 is the AP voltage at APD_{90}, and V_apd30 is the AP voltage at APD_{30}, t_apd90 is the time at which APD_{90} was measured, and t_apd30 is the time at which APD_{30} was measured. As triangulation quantifies the repolarisation rate, the numerical value (i.e. without the minus sign) was taken to quantify triangulation. Further, the sensitivity of APD to g_{K1} or g_{to} was simulated by changing the individual conductances in a graded manner and APD_{30} and APD_{90} recorded. The stimulus pulse required to elicit APs was 2 nA for 2 ms (CRN), 1.7 nA for 5 ms (Grandi), and 2 nA for 10 ms (KT). To verify the ion current alterations due to β-blocker remodelling, AP clamp simulations using AP recordings from our laboratory were performed to record ionic currents during realistic APs.

S1.3 APD restitution and ERP

APD restitution (APDr), using S1-S2 and dynamic pacing protocols, were computed in the cell models under control and β-blocker remodelled conditions. Since the cell models show prolonged rate dependent adaptation, stable APs were elicited using 25 conditioning pulses in all cases. S1-S2 APDr was computed [6] with 25 conditioning pulses (S1) at a pacing cycle length (PCL) of 1 s followed by a premature stimulus pulse (S2). APD_{90} and APD_{30} of the resultant premature AP excitation were measured. S1-S2 APDr curves were constructed by plotting APD_{90} and APD_{30} as functions of S2 interval. Maximal slopes of these curves were computed as an index known to influence re-entry [8]. Dynamic APDr was computed by pacing the cell models at various PCLs and measuring the APD_{90} and APD_{30} of the final 5 excitations. Cell effective refractory period (ERP) restitution was computed using the experimental pacing protocol as described in Workman et al. [9]. Briefly, a premature stimulus pulse (S2) with variable time delay (ΔT) was applied after 100 conditioning pulses (S1) at a given PCL. The minimum ΔT where the S2 produced peak AP amplitude of 80% of that of the last S1 AP was defined as the ERP. ERP was computed in a range of PCLs from 200 ms to 1000 ms to yield ERP restitution.

S1.4 Abrupt change of pacing rates

An abrupt change of pacing rate has been proposed as a pro-arrhythmic biomarker [10, 11], and was used in this study to quantify the anti-arrhythmic effects of β-blockade. The cell models were paced with a PCL of 1 s (1 Hz) for 500 beats, then at a faster pacing rate with PCL of 0.6 s (1.67 Hz) for 500 beats, and then for an additional 500 beats at a PCL of 1 s (1 Hz). The time series of the APD_{90} during the 0.6 s pacing was fitted by a mono-exponential function to quantify the APD_{90} adaptation [11], giving a time constant of adaptation. Under control conditions, the APD_{90} was seen to have a time constant of adaptation between 100 s to 260 s. This time constant has been observed to be approximately 300 s in human ventricle cells [11]. APD_{90} adaptation was defined as protracted when the adaptation time constant was abnormally longer than that observed experimentally [11] and in the control cell models, which relates to irregular APD adaptation dynamics and generation of ectopic excitations [11]. The time constants thus computed under control and β-blocker remodelled conditions were compared to quantify the anti-arrhythmic effects of β-blockade.

S1.5 Multi-cellular virtual tissue models

The multi-cellular tissue models were constructed as mono-domain spatially homogeneous reaction-diffusion systems with a partial differential equation formulation:

$$C_m \frac{\partial V_m}{\partial t} = -I_{ion} + D\nabla^2 V_m \qquad \text{Eq. (1)}$$

where C_m is the cell capacitance, V_m is the cell membrane potential, I_{ion} is the total ionic current flowing across the cell membrane, and D is the constant diffusion representing inter-cellular gap junctional coupling. D was taken to be 0.05 mm^2 ms^{-1} in CRN, 0.012 mm^2 ms^{-1} in Grandi, or 0.042 mm^2 ms^{-1} in KT to give a planar wave conduction velocity (CV) of 0.33 mm ms^{-1}. It may be appreciated that there is a large variation of measurements in atrial CV, but the CV implemented in this study falls in the measured range of 0.2–0.7 mm ms^{-1} in the atria [12, 13]. 1D virtual strands had a total length of 50 mm. The distance between the finite difference nodes was taken to be 0.2 mm in the 1D models. To be replaced with CRN, Grandi, KT (control and BB): 3D organ level simulations were conducted to evaluate the differences between the scroll wave behaviour with either type 1 AP (i.e. CRN basal AP), or type 3 APs (modified CRN as in Marshall et al. [5]). Although the CRN model's underlying ionic and intracellular mechanisms do not produce the experimentally observed type 3 APs, it has been demonstrated previously [5] that the CRN model can be modified to reproduce type 3 APs. Thus to simulate the triangular type 3 human atrial AP morphology, the I_{CaL} conductance (g_{CaL}) was reduced by 50% and the sustained outward K^+ current conductance (g_{sus}) was increased by 50%. The effects of β-blocker remodelling were then simulated as described above, i.e. by reducing g_{to} by 41% and g_{K1} by 34%. The modified CRN cell models were incorporated into the anatomically realistic 3D geometry of the human atria using a novel High Performance Computing cardiac simulation environment, Beatbox [14]. The 3D anatomical model has been developed in a previous study [15]. The inter-cellular distance in the 3D model was taken to be 0.33 mm uniformly in all directions.

S1.6 CV restitution and vulnerability window in 1D strands of atrial tissue

The rate dependence of the CV, or the CV restitution (CVr), was determined in 1D strands by stimulating one end of the strand at time S1, and then again at time S2. CVr was defined as CV of the AP evoked by S2 as a function of the inter-stimulus interval (SI = S2-S1 interval). The wavelength of a propagating AP was computed as the product of CV and APD_{90}. The temporal vulnerability of cardiac tissue was quantified by the width of a time window, during which a premature stimulus applied to the refractory tail of a preceding excitation wave produces uni-directional propagation[16, 17]. To compute the vulnerable window (VW), the 1D tissue mode was first conditioned with a S1 evoked excitation wave applied at one end of the strand. After a time delay, a S2 stimulus was applied in the middle of the strand. Depending on the time delay, the S2 evoked excitation wave can either propagates bi-directionally, or uni-directionally in the retrograde direction of the conditioning wave, or fail to propagate. The time interval during which the S2 evoked excitation wave propagates uni-directionally was defined as the VW.

S1.7 Initiation and simulation of spiral wave re-entry in 3D models

The 3D anatomical model was developed by Seemann et al. [15] in a previous study. In the 3D simulations, re-entrant spiral waves were initiated using an efficient phase distribution method [18]. Such a method ensures the initiation of spiral waves at desired locations in the model. The dependence of re-entry life span (LS) on the location of spiral wave initiation is thus eliminated. The initial scroll wave filament location was selected in the right atrial region, which does not have blood vessel opening or anatomical anomalies. Representative AP profiles from various locations in the 3D model were recorded to allow evaluation of localised pacing rates.

S1.8 Numerical algorithms

The cell model ordinary differential equations were solved using a variable time step explicit Runge-Kutta method with a maximum time step of 0.025 ms giving stable and accurate APs. The spatially extended 1D and 3D PDE models were solved using an implicit unconditionally stable finite difference approximation with appropriate multi-node finite difference approximations of the Laplacian. The space step was taken to be 0.2 mm in the 1D models. A reduction of space step (to 0.1 mm) affected the CV at less than 3% indicating accuracy of the implicit numerical scheme. The space step in the 3D was taken to be the anatomical model's spatial resolution of 0.33 mm, which gave stable solutions with a time step of 0.05 ms [6]. All computations used double precision arithmetic. Neumann boundary conditions at each surface of a boundary segment (1D), or voxel (3D) were implemented. Appropriate check pointing was implemented in all simulations requiring repetitive pacing. The cell and 1D simulations were carried out using parallel MATLAB. The 3D simulations were carried out using optimised MPI based parallel computation algorithms in Beatbox [14], which is a cardiac simulation software written in C. The UK National Supercomputing Service (HECToR) was used for the 3D simulations as well as large data visualisation. In the 3D simulations, a 5 s simulation took approximately 4 hours using 256 CPUs.

Supplementary Table

Table S1 Quantitative results of fitting the APD_{90} dynamics during 1.67 Hz pacing of cell models under control and β-blocker conditions. The formula used for fitting was taken to be $y = y_o + ae^{-t/t\_adaptation}$. Values of all evaluated constants (y_o, a, and $t_{\_adaptation}$) are given in the table below.

Model	$t_{\_adaptation}$ (s)	y_o (ms)	a (ms)
CRN (control, β-blocker)	258.3, 217.4	210.3, 312.9	36.6, 11.2
Grandi (control, β-blocker)	111.6, 96.4	284.4, 361.4	58.13, 72.4
KT (control, β-blocker)	255.8, 257.1	194.1, 246.3	23, 31

Supplementary Figures

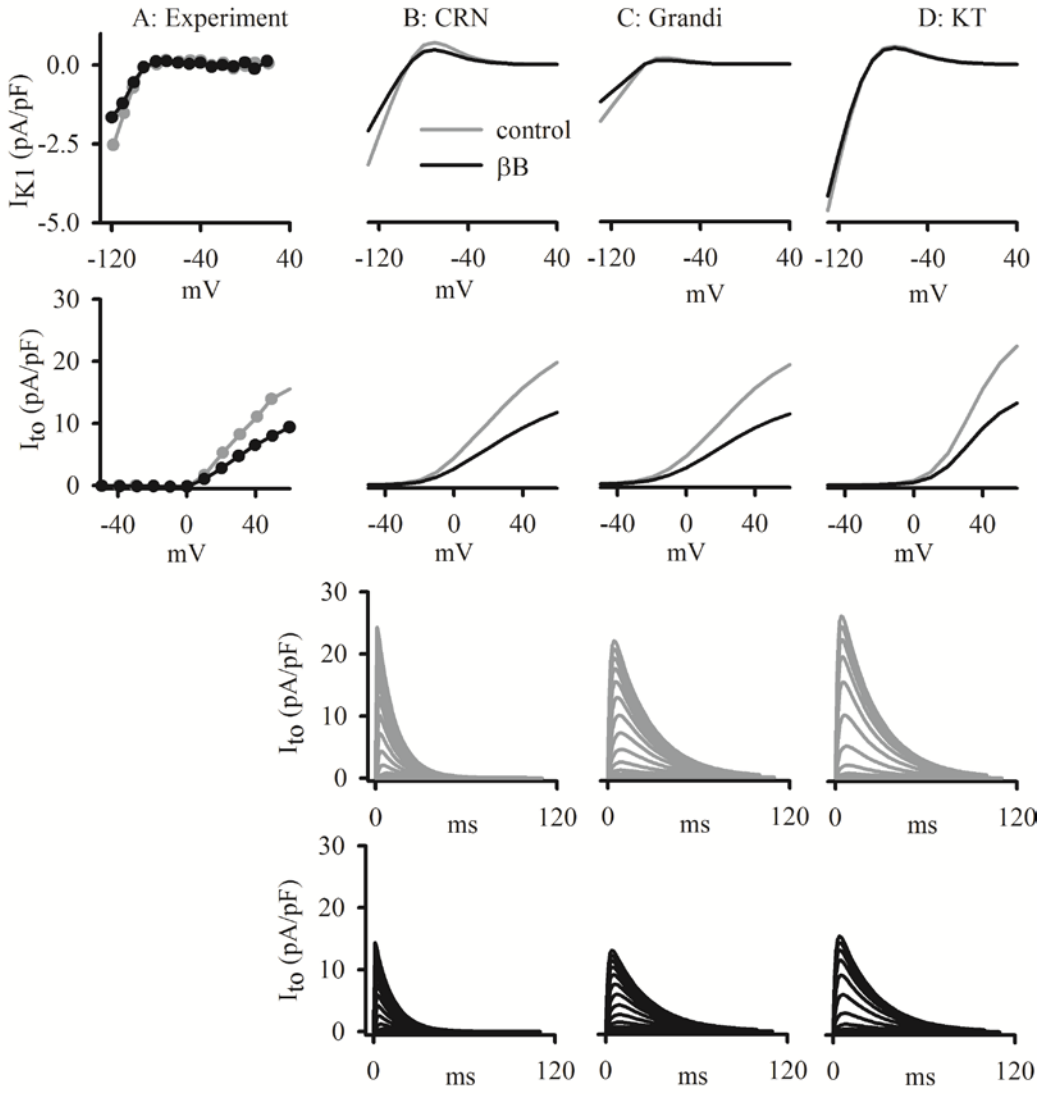

FIGURE S1 Voltage clamp simulation of I_{K1} and I_{to} current-voltage (I-V) relationships using experimental voltage clamp protocols [5]. In all panels, gray lines denote control data while black lines denote β-blocker data. Symbols in column A show experimental data. Column A shows experimental I-V data, while columns B-D show simulations using CRN, Grandi, and KT models respectively. Top row shows I-V for I_{K1} where g_{K1} is reduced by 34% in the CRN and Grandi models, while it is reduced by 10% in the KT model. Second row shows I-V for I_{to} where g_{to} is reduced by 41%. Third row shows simulated I_{to} current traces under control conditions, and bottom row shows simulated I_{to} current traces for β-blocker conditions.

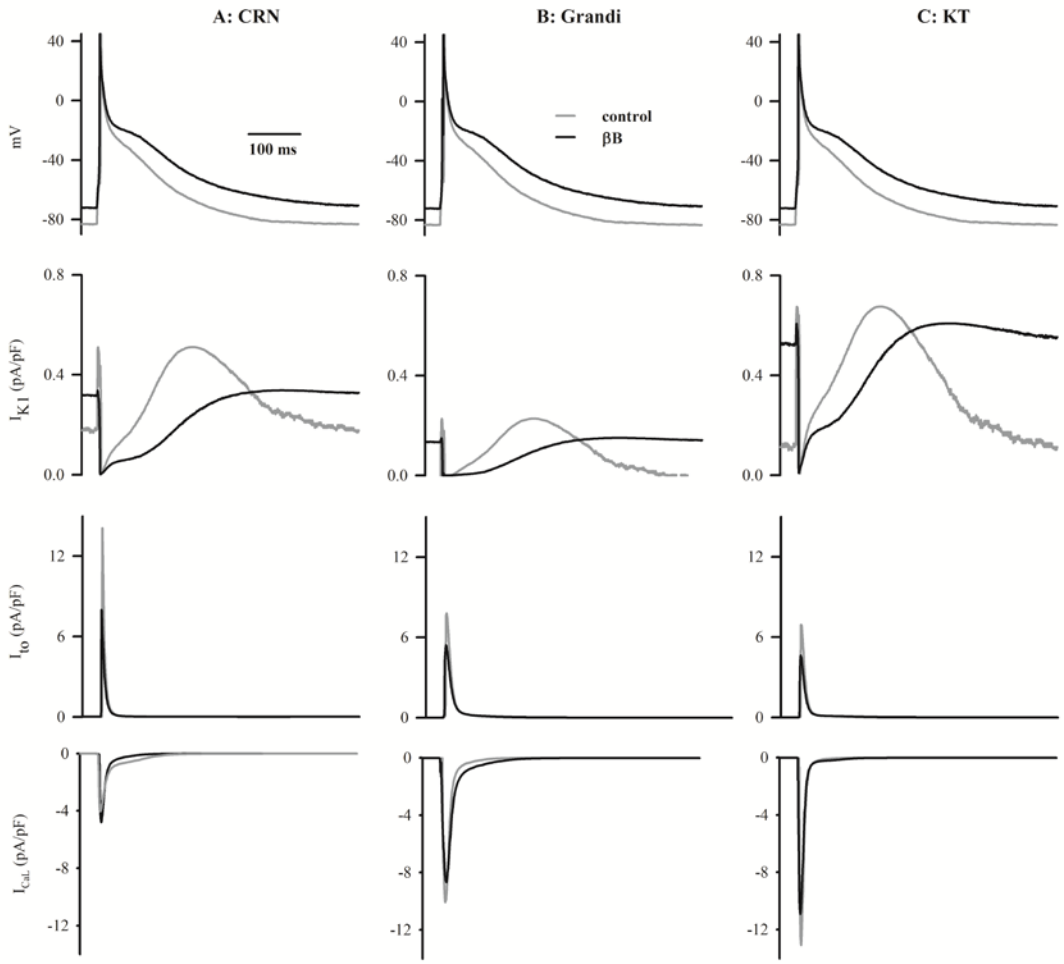

Figure S2 Ionic currents under AP clamp. AP recordings from our laboratory under β-blocker (solid line) and control conditions (gray line) are shown in the top row. I_{K1}, I_{to}, and I_{CaL} from CRN model (column A), Grandi (column B) and KT (column C) during AP clamp simulations.

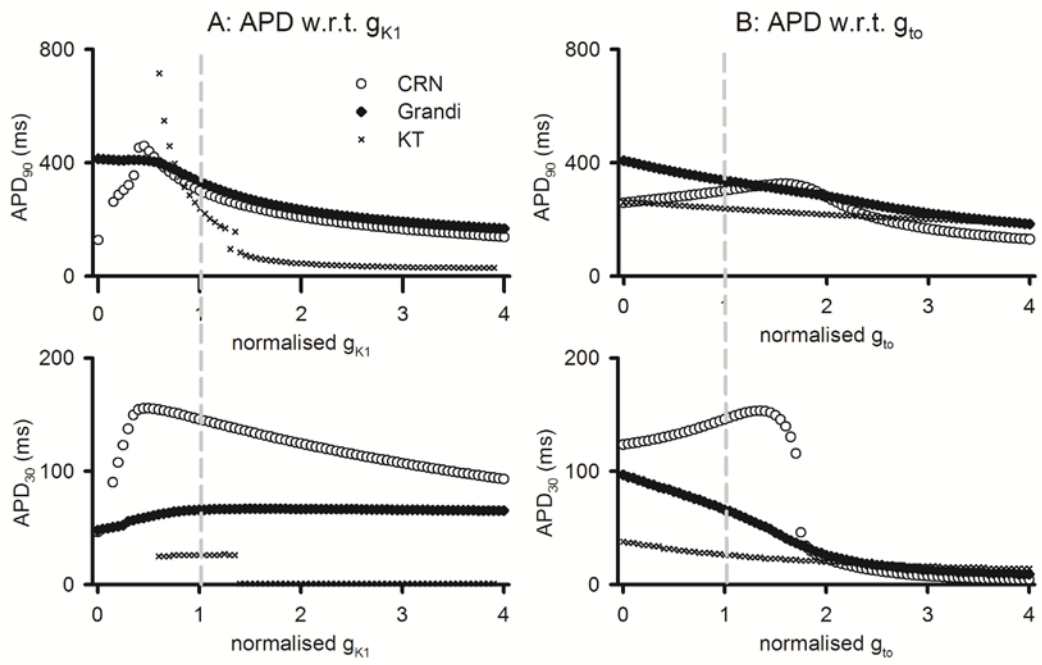

Figure S3 Dependence of APD_{90} (top row) and APD_{30} (bottom row) on g_{K1} (column A) and g_{to} (column B). In all panels, the conductances were normalised to basal values and are indicated by vertical dashed gray lines. CRN data are shown as empty circles, Grandi data by dots, ".", and KT data by "x". **A:** Effects of altering g_{K1} on APD_{90} (top left panel) and APD_{30} (bottom left panel) in the 3 cell models. **B:** Effects of altering g_{to} on APD_{90} (top right panel) and APD_{30} (bottom right panel) in the 3 cell models.

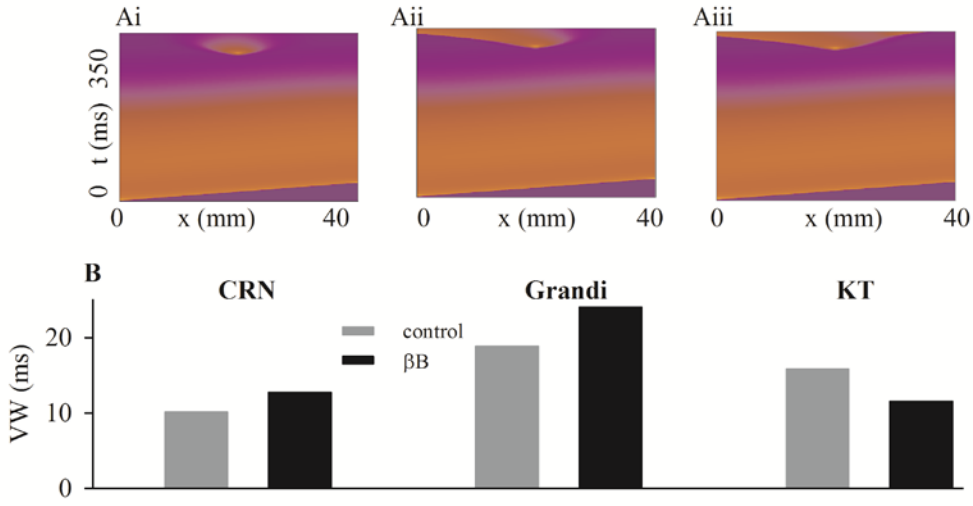

Figure S4 Temporal VW under control and β-blocker conditions. Top panels illustrate the pacing protocol. A conditioning pulse was followed by a premature stimulus in the middle of the 1D strand which either gave rise to no propagation (Ai), uni-directional propagation (Aii), or bi-directional propagation (Aiii). The VW computed in each of the three models is shown in the bar charts in the bottom panels under control (gray bars) and β-blocker (black bars) conditions. See Table 1 and main manuscript for quantitative results.

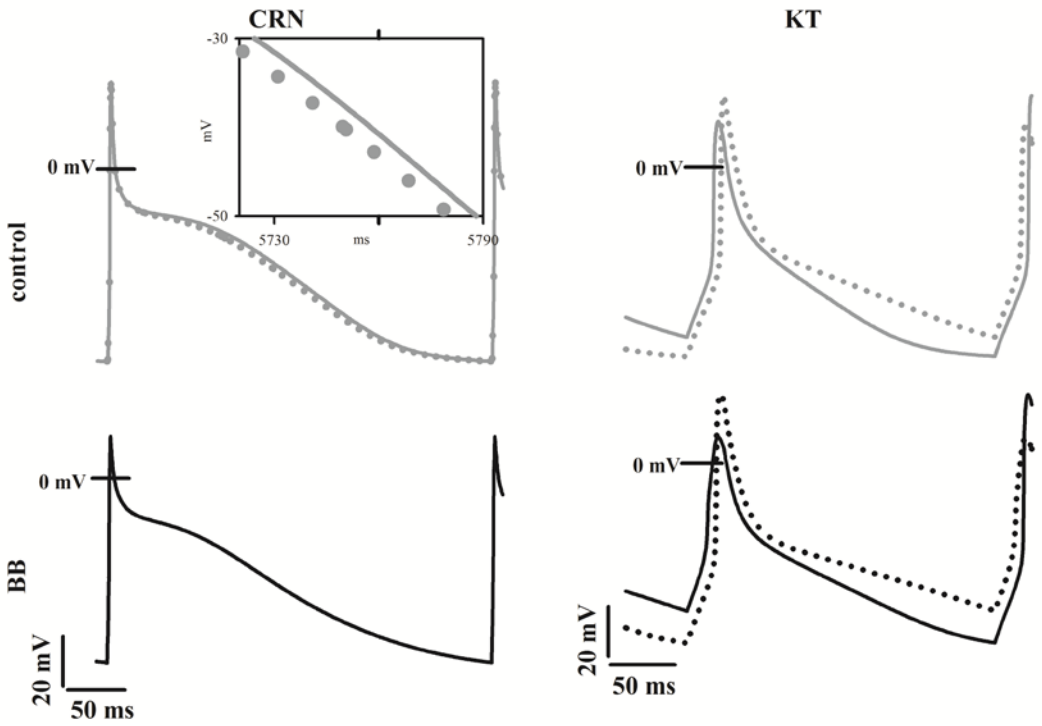

Figure S5 Superimposition of two consecutive AP profiles from dynamic APDr simulations demonstrating the beat to beat alternans. The penultimate AP is shown using solid lines and the final AP is shown using dotted lines in all panels. Top panels show data from control models (solid and dotted gray lines) while bottom panels show data from beta-B models (solid and dotted lines). The differences of the consecutive AP profiles in the CRN control case are highlighted in the inset of the CRN control case (top left panel).

References

[1] Courtemanche M, Ramirez RJ, Nattel S. Ionic mechanisms underlying human atrial action potential properties: insights from a mathematical model. *Am J Physiol* 1998; **275**: H301-21.

[2] Grandi E, Pandit SV, Voigt N, Workman AJ, Dobrev D, Jalife J, et al. Human atrial action potential and Ca2+ model: sinus rhythm and chronic atrial fibrillation. *Circ Res* 2011; **109**: 1055-66.

[3] Koivumaki JT, Korhonen T, Tavi P. Impact of sarcoplasmic reticulum calcium release on calcium dynamics and action potential morphology in human atrial myocytes: a computational study. *PLoS Comput Biol* 2011; **7**: e1001067.

[4] Dawodu AA, Monti F, Iwashiro K, Schiariti M, Chiavarelli R, Puddu PE. The shape of human atrial action potential accounts for different frequency-related changes in vitro. *Int J Cardiol* 1996; **54**: 237-49.

[5] Marshall GE, Russell JA, Tellez JO, Jhund PS, Currie S, Dempster J, et al. Remodelling of human atrial K(+) currents but not ion channel expression by chronic beta-blockade. *Pflugers Arch* 2012; **463**: 537-48.

[6] Kharche S, Garratt CJ, Boyett MR, Inada S, Holden AV, Hancox JC, et al. Atrial proarrhythmia due to increased inward rectifier current (I(K1)) arising from KCNJ2 mutation--a simulation study. *Prog Biophys Mol Biol* 2008; **98**: 186-97.

[7] Romero L, Carbonell B, Trenor B, Rodriguez B, Saiz J, Ferrero JM. Systematic characterization of the ionic basis of rabbit cellular electrophysiology using two ventricular models. *Prog Biophys Mol Biol*; **107**: 60-73.

[8] Xie F, Qu Z, Garfinkel A, Weiss JN. Electrical refractory period restitution and spiral wave reentry in simulated cardiac tissue. *Am J Physiol Heart Circ Physiol* 2002; **283**: H448-60.

[9] Workman AJ, Kane KA, Rankin AC. The contribution of ionic currents to changes in refractoriness of human atrial myocytes associated with chronic atrial fibrillation. *Cardiovasc Res* 2001; **52**: 226-35.

[10] Romero L, Pueyo E, Fink M, Rodriguez B. Impact of ionic current variability on human ventricular cellular electrophysiology. *Am J Physiol Heart Circ Physiol* 2009; **297**: H1436-45.

[11] Pueyo E, Husti Z, Hornyik T, Baczko I, Laguna P, Varro A, et al. Mechanisms of ventricular rate adaptation as a predictor of arrhythmic risk. *Am J Physiol Heart Circ Physiol* 2010; **298**: H1577-87.

[12] Colman MA, Aslanidi OV, Kharche S, Boyett MR, Garratt CJ, Hancox JC, et al. Pro-arrhythmogenic Effects of Atrial Fibrillation Induced Electrical Remodelling- Insights from 3D Virtual Human Atria. *J Physiol* 2013.

[13] Weber FM, Luik A, Schilling C, Seemann G, Krueger MW, Lorenz C, et al. Conduction velocity restitution of the human atrium--an efficient measurement protocol for clinical electrophysiological studies. *IEEE Trans Biomed Eng* 2011; **58**: 2648-55.

[14] McFarlane R, Biktasheva IV. Beatbox—A Computer Simulation Environment for Computational Biology of the Heart. In: Gelenbe E, Abramsky S and Sassone A eds. *Visions of Computer Science— BCS International Academic Conference*. London: British Computer Society 2008: 99-109.

[15] Seemann G, Hoper C, Sachse FB, Dossel O, Holden AV, Zhang H. Heterogeneous three-dimensional anatomical and electrophysiological model of human atria. *Philos Transact A Math Phys Eng Sci* 2006; **364**: 1465-81.

[16] Quan W, Rudy Y. Unidirectional block and reentry of cardiac excitation: a model study. *Circ Res* 1990; **66**: 367-82.

[17] Zhang H, Kharche S, Holden AV, Hancox JC. Repolarisation and vulnerability to re-entry in the human heart with short QT syndrome arising from KCNQ1 mutation--a simulation study. *Prog Biophys Mol Biol* 2008; **96**: 112-31.

[18] Biktashev VN, Holden AV. Reentrant waves and their elimination in a model of mammalian ventricular tissue. *Chaos* 1998; **8**: 48-56.

[19] Biktashev VN. Dissipation of the excitation wave fronts. *Phys Rev Lett* 2002; **89**: 168102.